ChemComm

Accepted Manuscript

This article can be cited before page numbers have been issued, to do this please use: K. Wang, L. Yang, Z. Wang, Y. Zhao, Z. Wang, L. Han, Y. Song and F. Pan, *Chem. Commun.*, 2018, DOI: 10.1039/C8CC07476C.

ROYAL SOCIETY OF CHEMISTRY

rsc.li/chemcomm

View Article Online
DOI: 10.1039/C8CC07476C

Journal Name

COMMUNICATION

Enhanced Lithium Dendrite Suppressing Capability Enabled by Solid-Like Electrolyte with Different-Sized Nanoparticles

Received 00th January 20xx,
Accepted 00th January 20xx

DOI: 10.1039/x0xx00000x

www.rsc.org/

Ke Wang, Luyi Yang*, Ziqi Wang, Yan Zhao, Zijian Wang, Lei Han, Yongli Song and Feng Pan*

A solid-like electrolyte (SLE-H) consisting of two different-sized ion conductors is prepared. Due to the higher packing density, SLE-H exhibits improved ionic conductivity. During Li plating/stripping, larger nanoparticles serve as physical barricades for dendrite growth, while smaller nanoparticles facilitate better contact with Li. Consequently, SLE-H demonstrates superior dendrite suppressing capability.

Lithium-ion batteries (LIBs) have dominated the market of portable low-power electronic devices over a long period of time, however, issues such as low energy density and safety hazards have limited their applications in high-power electronic devices.[1–4] Consequently, solid-state batteries (SSBs) have attracted much attentions as they are able to avoid the potential safety risks of using flammable liquid electrolytes. More importantly, solid-state electrolytes are promising candidates for the use Li metal anode, which has a much higher specific capacity (3829 mAh g^{-1}) compared with commercially used graphite (372 mAh g^{-1}) anode, leading to a higher energy density.[5] These advances have made SSBs very promising candidates for future energy storage.[6,7] However, the interfacial issues between the electrodes and the solid-state electrolytes (SSEs) are huge obstructions which prohibit the practical application of SSBs.[8,9] On the one hand, the poorly-contacted interfaces between SSEs and cathode materials have severely restricted the active loading and energy density owing to the sluggish Li-ion transfer process;[10,11] on the other hand, the unstable interfaces between Li anode and SSEs also lead to dendrite formation.[12] Therefore, solving the interfacial issue is essential for further development of SSBs. In order to modify the interface between Li and SSE, researchers have used different approaches such as applying lithiophilic coatings[13–15] or using polymers as buffer layers;[16,17] whereas the interfacial contact between SSEs and cathode materials are normally reduced by sintering method. Previously, by loading Li-contained ionic liquid (Li-IL) to metal-organic frameworks (MOFs) with inter-connected channels, we have proposed a solid-like electrolyte (SLE).[18] MOFs are chosen as electrolyte hosts not only for their porous structures, but also for the simple preparation procedures with controllable morphologies[19]. Distinguished from the traditional SSEs with limited contact area between solid particles, SLE provides nano-wetted interfaces to promote the Li-ion transport between the electrolyte and the electrode.

Herein, a novel SLE with hybrid-sized of nanoparticles (SLE-H) is proposed, where small SLE nanoparticles (about 20 nm) are filled in the voids between large SLE nanoparticles (about 200 nm), resulting a more closely internal stacking. As a result, comparing to SLE only consists of large (SLE-L) and small (SLE-S) nanoparticles, SLE-H shows higher room temperature ionic conductivity (3.3×10^{-4} S cm^{-1}). More importantly, it is also found that SLE-H exhibits a superior ability to prevent short-circuiting during Li plating/stripping process. The result can be ascribed to the unique properties of SLE-H: the smaller nanoparticles facilitate a larger contact area with Li metal, leading to a more homogenous Li plating/stripping; while larger nanoparticles physically barricade the growth of Li dendrite. In addition, by coupling SLE-H with the $LiFePO_4$ and $LiCoO_2$ cathode materials, good cycling performance and rate capability are also obtained with high active loadings of 12.4 and 10.7 mg cm^{-2}, respectively. By studying the effects of particle sizes on the ionic conductivity as well as Li dendrite suppression, this work provides guidance on the design of high-performance solid state electrolytes for Li metal batteries.

The morphologies of different-sized UIO-66 (standing for Universitetet I Oslo-66) nanoparticles can be observed from the scanning electron microscopy (SEM) image in **Figure 1a** and **Figure 1b**. Both samples exhibit uniformly distributed particle sizes and similar particle

School of Advanced Materials, Peking University Shenzhen Graduate School, Shenzhen 518055, China
Email: yangly@pkusz.edu.cn
Email: panfeng@pkusz.edu.cn
Electronic Supplementary Information (ESI) available: [Experimental details and supplementary figures]. See DOI: 10.1039/x0xx00000x

View Article Online
DOI: 10.1039/C8CC07476C

morphologies. Since Li-IL acts as the Li^+ conductive guest, the degree of Li-IL saturation in the pores of UIO-66 host directly determines its ionic conductivity of SLE.[20] Therefore, it is necessary to find the optimal weight ratio of Li-IL and UIO-66. As shown in **Figure S1a**, by adding 1.0, 1.2 and 1.4 mL of Li-IL into 1.0 g of mixed UIO-66 nanoparticle host, room temperature ionic conductivities of 8.1×10^{-5} S cm^{-1}, 3.3×10^{-4} S cm^{-1} and 6.9×10^{-4} S

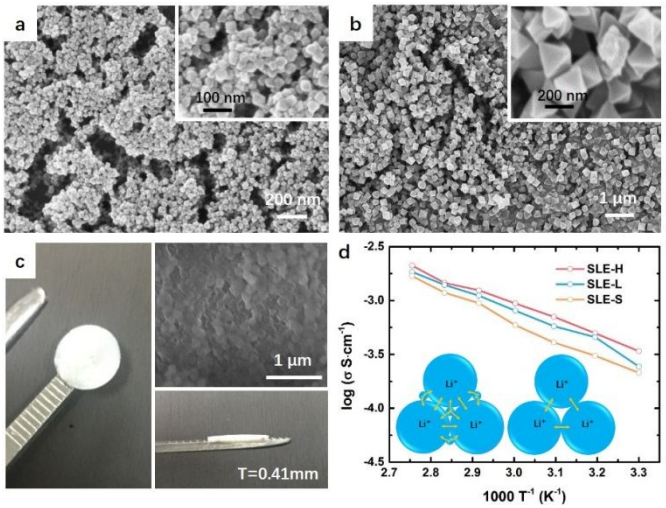

Figure 1. SEM images of the synthesized a) UIO-66 (about 20 nm) and b) UIO-66 (about 200 nm) host (the inset shows SEM image at a higher magnification). c) The front and side pictures and SEM image of the hybrid UIO-66 pressed into a pellet. d) Arrhenius plots for the ionic conductivity of Li-IL@UIO-66 with different UIO-66 sizes (the inset shows schematic illustrations of Li-ion transfer in SLEs with higher packing density and lower packing density).

cm^{-1} are obtained. Although the ionic conductivity increased as a result of higher Li-IL content, the nanoparticles loaded with 1.4 mL of Li-IL start to agglomerate (shown in **Figure S1b, S1c and S1d**), indicating over saturation of Li-IL. Therefore, the amount of 1.2 mL, at which the saturation of Li-IL can be achieved in UIO-66, is adopted for the following measurements. The crystal information of as-prepared UIO-66 nanoparticles with different sizes is examined via X-ray diffraction (XRD). As shown in **Figure S2**, both XRD patterns are consistent with previously reported crystal structures. [20] It can be also seen that the XRD patterns of MOF particles remain almost unchanged after loading with Li-IL, suggesting good chemical compatibility between them. In addition, according to the results of N_2 adsorption/desorption experiments (details are shown in **Figure S3**), the BET specific surface area and BJH pore volume of the hybrid UIO-66 nanoparticles are measured to be 787.1 m^2 g^{-1} and 0.6 cm^3 g^{-1}, respectively. These values plummet to 17.5 m^2 g^{-1} and 0.05 cm^3 g^{-1} after the impregnation of Li-IL. The significant decreases of the BET surface area and pore volume also indicate that the pores of the hybrid UIO-66 have been almost filled by Li-IL. As shown in **Figure 1c**, after being pressed into a pellet with the thickness of approximately 0.4 mm, SLE-H demonstrates not only compact particle packing without visible pin-holes, but also the appearance of solid-state electrolytes. In addition, SLE-H shows higher density (1.70 g cm^{-3}) compared with SLE-L (1.58 g cm^{-3}) and SLE-S (1.53 g cm^{-3}), suggesting that SLE particles are more densely packed in SLE-H pellet because **s**mall SLE nanoparticles (about 20 nm) are filled in the voids between large SLE nanoparticles (about 200 nm) to generate a more closely internal stacking.

In order to explore the role of different particle sizes on the ionic conductivity of SLE, electrochemical impedance spectra of SLE-H, SLE-L and SLE-S at temperatures from 30 to 90 ºC are shown in **Figure S4a**, **Figure S4b** and **Figure S4c**, respectively. The corresponding Arrhenius curves are presented in **Figure 1d**. It can be seen that the SLE-H exhibits the highest room-temperature ionic conductivity (3.3×10^{-4} S cm^{-1}), followed by SLE-L (2.45×10^{-4} S cm^{-1}) and SLE-S (2.14×10^{-4} S cm^{-1}), which shows the same trend with the pellet densities of SLE. Therefore, as demonstrated in the inset of **Figure 1d**, the higher ionic conductivity of SLE-H (left) can be ascribed to the higher packing density of the SLE particles, which provides extra channels for Li-ion to transfer.

The lithium ion transference number (t_{Li+}) of SLE-H is also measured (detailed data shown in **Figure S5**) to be 0.25, which is higher than that of Li-IL (0.18). This is consistent with the work reported previously, where it is shown that porous MOF species are able to control the migration of large-sized anions, leading to a higher t_{Li+}.[21] In order to evaluate the electrochemical window of SLE-H, cyclic voltammetry (CV) and linear sweep voltammetry (LSV) are carried out. As shown in **Figure S6**, by sweeping the voltage positively, the decomposition voltage of SLE-H is measured to be 5.2 V vs Li/Li^+, which is sufficient for the application of high-voltage cathode materials. Then the cyclic voltammogram of SLE-H between -0.5 and 3 V vs Li/Li^+ indicates a stable Li plating/stripping process.

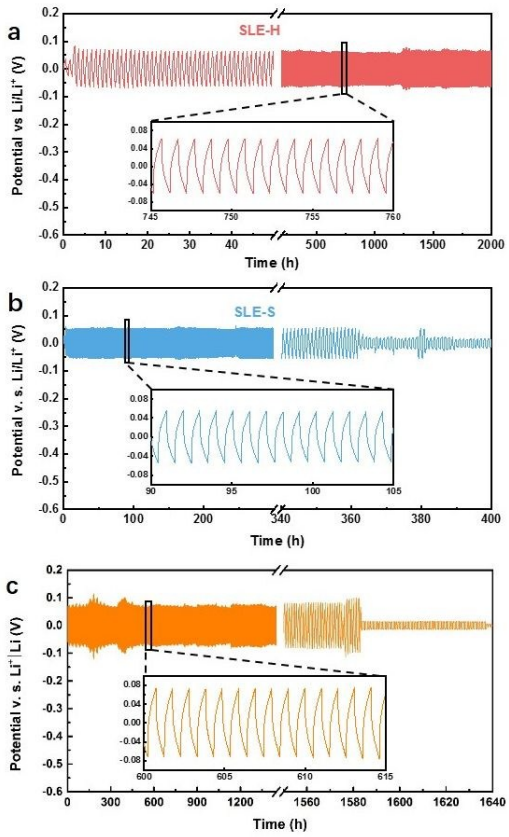

Figure 2. Li|SLE-S| density o

View Article Online
DOI: 10.1039/C8CC07476C

To evaluate the stability of the SLEs during Li plating/stripping for lithium metal SSBs, Li|SLE|Li symmetric cells are assembled for the constant current Li plating/stripping test at a current density of 0.1 mA cm^{-2} with areal capacity of 0.05 mA cm^{-2} for each step at room temperature. As shown in **Figure 2a**, SLE-H exhibits smooth voltage profile for over 2000 hours cycling without no short-circuits. In comparison, as shown in **Figure 2b** and **Figure 2c**, short-circuits are observed for SLE-L and SLE-S after cycling for 1585 and 363 hours, respectively. These results imply stronger Li-dendrite suppressing capability of SLE-H during continuous Li plating/stripping process. In addition, SEM morphology of the Li metal surface after Li plating/stripping for 100 cycles in Li|SLE-L|Li, Li|SLE-S|Li and Li|SLE-H|Li symmetric cell are shown in **Figure 3a**, **Figure 3b** and **Figure 3c**, respectively. It can be clearly observed that much smoother Li surface is resulted from SLE-H compared to SLE-S and SLE-L. This difference can be attributed to the synergic combination of large and small particles. On the one hand, the large SLE particles contact poorly with Li metal anode, resulting in high localized current densities and inhomogeneous Li plating/stripping (shown in **Figure 3d**); on the other hand, SLE-S is more likely to be penetrated by Li dendrite due to the higher mobility of smaller SLE particles (shown in **Figure 3e**). Therefore, for SLE-H the smaller particles increase the contact area with Li anode, which facilitates a "softer" contact with Li and leads to a more homogeneous Li plating/stripping while the larger SLE particles could more effectively barricade the propagation of Li dendrites (shown in **Figure 3f**). For comparison, **Figure S7** shows that in a cell using Li-IL electrolyte with commonly used glassfiber separator, short-circuiting occurs after only 85 h, which is much faster than the cells using SLEs, indicating improved dendrite suppressing capability for SLEs. In order to probe the stability of UIO-66 to Li anode, SLE-H pellet was examined by XRD after cycling. As shown in **Figure S8**, the XRD patterns of pristine SLE-H and cycled SLE-H are

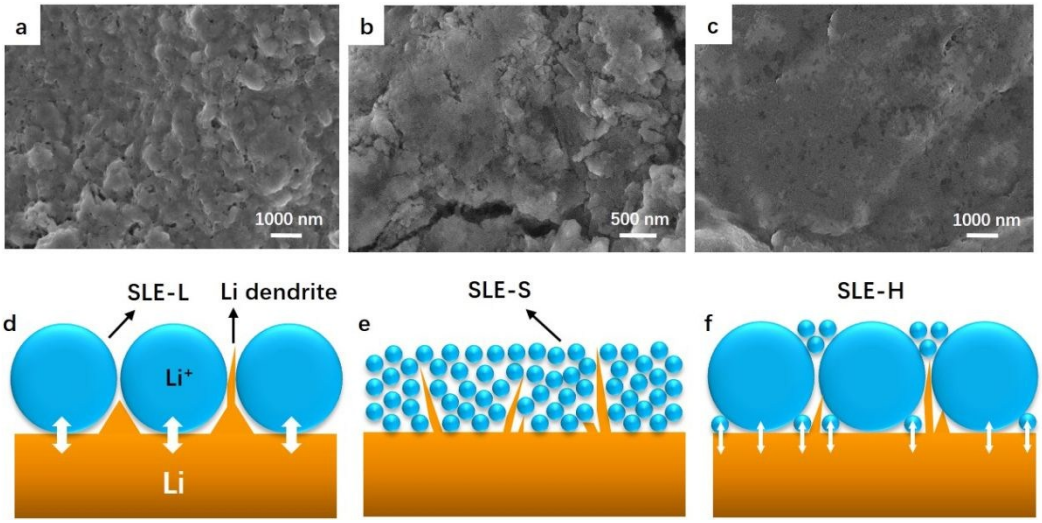

Figure 3. a, b, c) SEM morphology of the Li metal surface after Li
H|Li symmetric cell, respectively. Schematic illustrations of Li pla
Li/SLE-S and f) Li/SLE-H.

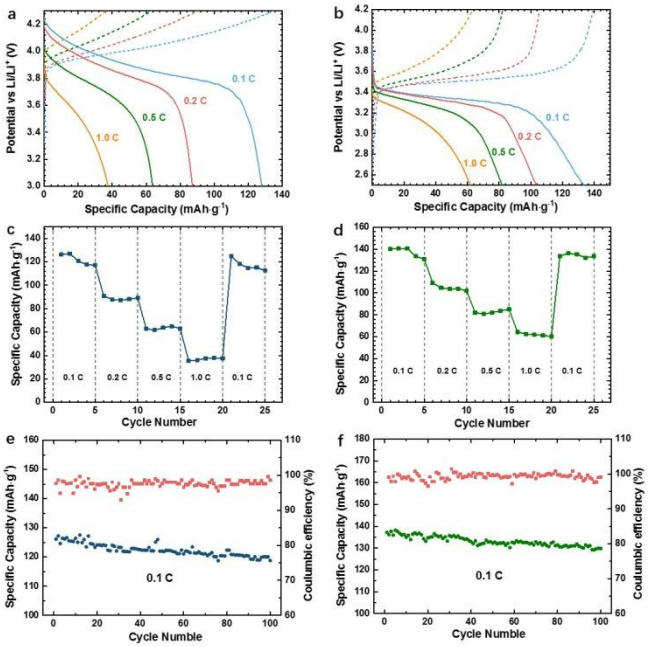

Figure 4. a) Charge-discharge profiles under different current rates, b) the rate capability, and c) the cycle performance at 0.1 C with Coulombic efficiency of the $LiCoO_2$ SSBs. d) Charge-discharge profiles under different current rates, e) the rate

View Article Online
DOI: 10.1039/C8CC07476C

almost identical, indicating no phase transition or degradation during the long-term cycling.

Ionic transport within cathode is a limiting factor for traditional solid-state batteries due to the high interfacial impedance. Herein, SLE-H is mixed with cathode materials in order to solve the ionic transport issues. The cell configuration is presented in **Scheme S1**, where the active materials ($LiCoO_2$ and $LiFePO_4$) are mixed with acetylene black and SLE-H to form the cathode layer, where carbon

and SLE particles are responsible to generate networks for electron and Li-ion conduction, respectively. The cathode layer is then pressed onto SLE-H pellet and then assembled with Li metal anode. **Figure S9** and **Figure S10** exhibit the SEM image and corresponding energy dispersive spectra (EDS) of the cross-section morphology of the cathode layer and SLE-H layer. It can be observed that electrochemical active particles are evenly distributed in the cathode layer, which can be distinguished from the electrolyte layer by a well-defined boundary. The resultant $LiCoO_2$ and $LiFePO_4$ areal

loadings for the batteries are 10.7 and 12.4 mg cm^{-2}, respectively. The voltage profiles of the cells under different C-rates are exhibited in **Figure 4a** and **Figure 4b**. Acceptable voltage polarizations can be seen in both cells, which can be attributed to the high areal loading. The corresponding rate performances are presented in **Figure 4c** and **Figure 4d**. For $LiCoO_2$ based cell, discharge capacities of 126 mA h g^{-1}, 90 mA h g^{-1}, 62 mA h g^{-1} and 38 mA h g^{-1} are obtained at 0.1 C, 0.2 C, 0.5 C and 1 C, respectively at room temperature; whereas for $LiFePO_4$ based cell, discharge capacities of 140 mA h g^{-1}, 103 mA h g^{-1}, 81 mA h g^{-1} and 62 mA h g^{-1} are achieved under the same testing conditions. The galvanostatic charge/discharge long-term cycling performances of the cells are carried out at 0.1 C at room temperature. As presented in **Figure 4e**, an initial discharge capacity of 129 mA h g^{-1} is achieved for $LiCoO_2$|SLE-H|Li cell; after 100 cycles, a capacity of 122 mA h g^{-1} (94.6 % capacity retention) can be achieved. For $LiFePO_4$|SLE-H|Li cell (shown in **Figure 4f**), the discharge capacity decreases from 137 mA h g^{-1} to 130 mA h g^{-1} over 100 cycles, which results in a capacity retention of 94.8 %. Both cells also exhibit high Coulombic efficiencies, suggesting that side reactions are kept at a relatively low level. The cycling results indicate that SLE-H not only shows excellent stability towards Li metal anode, but also exhibits good compatibility with commonly used cathode materials at room temperature.

In summary, a novel solid-like electrolyte (SLE-H) is designed and synthesized by mixing two different sized MOF UIO-66 nanoparticles impregnated with Li-IL. By increasing the packing density with mixture of different sized nanoparticles, more Li-ion transport channels are resulted, which lead to an improved ionic conductivity at room-temperature can be achieved (3.3×10^{-4} S cm^{-1}). More importantly, SLE-H also exhibited superior ability to suppress the dendrite formation and growth due to the synergic combination of two different sized SLE: the small SLE particles facilitate a better contact with Li metal, which enables homogeneous Li plating/stripping; while the large SLE particles mechanically barricade the propagation of Li dendrite. Finally, by coupling SLE-H with commercially used cathode materials such as $LiFePO_4$ and $LiCoO_2$, good rate performances and long-term cycling stability can also be achieved. The unique design of SLE provides useful guidance for other battery system such as inorganic solid electrolyte based batteries, where interface issues are limiting factors for their practical applications.

This research was financially supported by the National Key R&D Program of China (2016YFB0700600), the Guangdong Innovation Team Project (No. 2013N080) and Shenzhen Science and Technology Research Grants (JCYJ20160531141048950, JCYJ20151015162256516, JCYJ20150729111733470 and JCYJ20160226105838578)

Conflicts of interest

There are no conflicts to declare.

Notes and references

1 M. V. Reddy, G. V. Subba Rao and B. V. R. Chowdari, *Chem. Rev.*, 2013, **113**, 5364–5457.
2 W. Li, B. Song and A. Manthiram, *Chem. Soc. Rev.*, 2017, **46**, 3006–3059.
3 P. G. Bruce, S. A. Freunberger, L. J. Hardwick and J.-M. Tarascon, *Nat. Mater.*, 2011, **11**, 19.
4 Y. Liu, P. He and H. Zhou, *Adv. Energy Mater.*, 2018, **8**, 1–22.
5 L. Fan, S. Wei, S. Li, Q. Li and Y. Lu, *Adv. Energy Mater.*, 2018, **1702657**, 1–31.
6 X. Yao, B. Huang, J. Yin, G. Peng, Z. Huang, C. Gao, D. Liu and X. Xu, *Chinese Phys. B*, , DOI:10.1088/1674-1056/25/1/018802.
7 C. Sun, J. Liu, Y. Gong, D. P. Wilkinson and J. Zhang, *Nano Energy*, 2017, **33**, 363–386.
8 L. Chen, Y. Li, S. P. Li, L. Z. Fan, C. W. Nan and J. B. Goodenough, *Nano Energy*, 2018, **46**, 176–184.
9 Y. Shen, Y. Zhang, S. Han, J. Wang, Z. Peng and L. Chen, *Joule*, 2018, 1–16.
10 K. K. Fu, Y. Gong, B. Liu, Y. Zhu, S. Xu, Y. Yao, W. Luo, C. Wang,

View Article Online
DOI: 10.1039/C8CC07476C

S. D. Lacey, J. Dai, Y. Chen, Y. Mo, E. Wachsman and L. Hu, *Sci. Adv.*, 2017, **3**, 1–12.

11 X. Yao, D. Liu, C. Wang, P. Long, G. Peng, Y. S. Hu, H. Li, L. Chen and X. Xu, *Nano Lett.*, 2016, **16**, 7148–7154.

12 M. D. Tikekar, S. Choudhury, Z. Tu and L. A. Archer, *Nat. Energy*, 2016, **1**, 16114.

13 X. Han, Y. Gong, K. Fu, X. He, G. T. Hitz, J. Dai, A. Pearse, B. Liu, H. Wang, G. Rubloff, Y. Mo, V. Thangadurai, E. D. Wachsman and L. Hu, *Nat. Mater.*, 2017, **16**, 572–579.

14 W. Luo, Y. Gong, Y. Zhu, Y. Li, Y. Yao, Y. Zhang, K. K. Fu, G. Pastel, C. F. Lin, Y. Mo, E. D. Wachsman and L. Hu, *Adv. Mater.*, 2017, **29**, 1–7.

15 C. Wang, Y. Gong, B. Liu, K. Fu, Y. Yao, E. Hitz, Y. Li, J. Dai, S. Xu, W. Luo, E. D. Wachsman and L. Hu, *Nano Lett.*, 2017, **17**, 565–571.

16 L. Yang, Z. Wang, Y. Feng, R. Tan, Y. Zuo, R. Gao, Y. Zhao, L. Han, Z. Wang and F. Pan, *Adv. Energy Mater.*, 2017, **7**, 1–9.

17 W. Zhou, S. Wang, Y. Li, S. Xin, A. Manthiram and J. B. Goodenough, *J. Am. Chem. Soc.*, 2016, **138**, 9385–9388.

18 Z. Wang, R. Tan, H. Wang, L. Yang, J. Hu, H. Chen and F. Pan, *Adv. Mater.*, 2018, **30**, 1–7.

19 S. Wang, W. Morris, Y. Liu, C. M. McGuirk, Y. Zhou, J. T. Hupp, O. K. Farha and C. A. Mirkin, *Angew. Chemie - Int. Ed.*, 2015, **54**, 14738–14742.

20 K. Fujie, R. Ikeda, K. Otsubo, T. Yamada and H. Kitagawa, *Chem. Mater.*, 2015, **27**, 7355–7361.

21 S. Bai, Y. Sun, J. Yi, Y. He, Y. Qiao and H. Zhou, *Joule*, , DOI:10.1016/j.joule.2018.07.010.